Nanometer-scale test of the Tung model of Schottky-barrier height inhomogeneity

H.-J. Im,* Y. Ding, and J. P. Pelz
Department of Physics, The Ohio State University, Columbus, Ohio 43210

W. J. Choyke
Department of Physics and Astronomy, University of Pittsburgh, Pittsburgh, Pennsylvania 15260
(Received 26 January 2001; published 25 July 2001)

Tung has shown [Phys. Rev. B **45**, 13 509 (1992)] that a range of ''nonideal'' behaviors observed in metal/semiconductor (MS) Schottky diodes could be quantitatively explained by assuming that specific microscopic distributions of nanometer-sized ''patches'' of reduced barrier height exist at the MS interface. Here we report a *simultaneous* microscopic and macroscopic test of this model as applied to metal/6*H*-SiC Schottky diodes, by (1) measuring the nm-scale barrier-height distribution (BHD) of particular Schottky diodes using ultrahigh vacuum (UHV) ballistic electron emission microscopy (BEEM), (2) extending the Tung model to calculate the expected nm-scale BHD for particular parameter values, and (3) quantitatively relating the measured nm-scale BHD of a particular Schottky diode to its macroscopic *I-V* characteristic. Our studies indicate that (1) for relatively ideal diodes, both the microscopic and macroscopic behaviors are explained well by the Tung model with a large coverage ($>5\%$) of shallow patches, (2) the measured BHDs are nearly identical for relatively ideal and highly nonideal diodes, and (3) a simple Tung model can account for highly nonideal behavior only by assuming an unphysical patch distribution in which the excess current is dominated by a few patches in the extreme tail of the patch distribution. Our measurements instead suggest that all the diodes contain a broad ''intrinsic'' distribution of shallow patches, while the large excess current in highly nonideal diodes is due to a few large defects of *extrinsic* origin. This last conclusion is consistent with a recent study by Skromme and co-workers [J. Electron. Mater. **29**, 376 (2000)].

DOI: 10.1103/PhysRevB.64.075310 PACS number(s): 73.40.Ns, 73.40.Sx

I. INTRODUCTION

Electrical transport across metal/semiconductor (MS) contacts is of great technological importance and has been the subject of long-standing scientific controversy.[1,2] Recent interest in wide-bandgap materials such as SiC and GaN increases the demand for better understanding and control of the metal contacts, for making both good Ohmic contacts (for large current injection applications) and rectifying Schottky contacts (for field effect and other devices).[3,4] However, fabricated Schottky contacts on these wide-bandgap materials often exhibit significant device-to-device variations and/or ''nonideal'' behavior in measured current-voltage (*I-V*) characteristics. It is clearly important to understand the physical origin of such nonideal behavior so that it can be controlled in future device applications. Freeouf *et al.*[5] in 1981, as well as Ohdomari *et al.*[6] and Bastys *et al.*[7] in the late 1980's, demonstrated that if small interfacial ''patches'' with reduced *local* Schottky-barrier height (SBH) exist and are of size comparable to or less than the semiconductor Debye length, then a so-called ''potential pinch-off'' would occur within the patches. This would result in a voltage-dependent variation in the local barrier height and could explain in a natural way a variety of observed nonideal behavior, including observations of a diode ''ideality factor'' that was larger than the expected ideal factor or $n \cong 1$. In 1991, Tung further developed the ideas and showed[8] that this nonideal behavior could be quantitatively explained by assuming specific distribution of nanometer-scale interfacial patches of reduced SBH. Since then several authors have been able to account for much of the observed nonideal behavior by assuming certain distributions of microscopic barrier heights for the different diodes,[8–13] and have pointed out that this would also explain the strong correlation that is often observed between the ''effective'' barrier height and the ideality factor measured on sets of diodes.[12] There is experimental evidence[14–17] that nm-sized lateral variations in SBH may exist, at least in certain MS systems. Olbrich *et al.*[11,16] has recently shown that potential pinch-off effect can be observed near intentionally introduced low-barrier height areas in Au/Co/GaAsP diodes, and that these low-barrier areas correlate well with the effective barrier height of the entire diode.

To date, however, there has been no attempt to *directly* relate naturally occurring nm-scale variations in the SBH of a particular diode to the nonideal ''macroscopic'' behavior of the *I-V* characteristic of that diode. It should be possible to do this, since nm-scale patches can be measured and quantified by the nm-resolution technique of ballistic electron emission microscopy (BEEM).[18] This would help determine whether the Tung model (or some other mechanism) is mostly responsible for observed nonidealities in particular kinds of fabricated Schottky diode structures. Such a comparison of nm-scale and macroscopic behavior is important to do, particularly since a recent study by Skromme *et al.*[19] of Schottky diodes on 4*H*-SiC suggests that the nonideal behavior in that system may in fact be due mostly to a few large (μm-scale) pathological defects, rather than to a more ''homogeneous'' distribution of nm-scale patches. Understanding the true physical origin of the nonideal behavior is essential for future efforts to reduce and eliminate it.

Here we report direct nm-scale measurements and model-

ing designed to *quantitatively* test the limits of the Tung model for explaining nonideal diode behavior in Pd/6*H*-SiC contacts. We do this by (1) using BEEM to sample the nm-scale barrier-height distributions (BHDs) over the surface of particular Schottky diodes, (2) using the Tung model to calculate *both* the expected macroscopic diode *I-V* curves and the expected nm-scale BHDs that should result from specific ''patch parameter'' distributions, and (3) comparing the measured BHDs to the calculated BHDs to determine which patch parameter distributions could possibly be present in actual, nonideal Schottky diodes. Our results are a bit surprising. For a nearly ideal diode ($n<1.1$ over a wide voltage range), both the nm-scale BEEM measurements and the diode *I-V* curve are consistent with a broad distribution of shallow patches that cover a large fraction (>5%) of the sample surface. However, for a diode with significant nonidealities, our measurements rule out the possibility that the extreme nonidealities are caused by a broad distribution of patches that cover a significant fraction (>1%) of the diode area. The nm-scale measurements cannot directly rule out the possibility that the nonidealities are caused by deeper patches that cover a much smaller fraction of the diode area, since these patches would likely be *missed* by BEEM measurements that can only sample a small fraction of the diode area. However, a more detailed analysis of the Tung model in the small-coverage limit indicates that most of the nonideal behavior would be due to *an extremely small number* (on average $\ll 1$ in an entire device) of very ''deep'' patches in the extreme tail of a Gaussian patch-parameter distribution. We believe that a more likely explanation is that the nonideal behavior in this case is due to a few large defects of *extrinsic* origin, as suggested in recent studies by Skromme *et al.*[19]

II. EXPERIMENTAL PROCEDURE

The SiC wafer consisted of a Si-terminated 6*H*-SiC (0001) epilayer grown on a 6*H*-SiC substrate, and was chemically cleaned by solvent ultrasonic bath followed by repeated ultraviolet ozone oxidation/HF etching cycles. Details of the cleaning procedure are discussed elsewhere.[20] Both the epilayer and substrate are *n*-doped with concentrations of $N_D=3\times10^{15}\,\mathrm{cm}^{-3}$ and $1\times10^{18}\,\mathrm{cm}^{-3}$, respectively. The sample was then introduced into ultrahigh vacuum (UHV), and a number of 0.5-mm-diameter Schottky diodes were made by depositing a 6-nm-thick Pd film through a shadow mask using electron-beam evaporation. The substrate was then passed into an adjacent UHV analysis chamber, where a 0.1 mm diameter Au wire contacted and measured the diodes one at a time. The SiC substrate served as the common back contact for all the diodes. All ''macroscopic'' diode *I-V* measurements as well as the nm-scale BEEM measurements were done *in situ* at room temperature.

III. RESULTS AND DISCUSSION

A. Measurements

The macroscopic diode *I-V* measurements of the various diodes exhibit a variety of behaviors, ranging from nearly

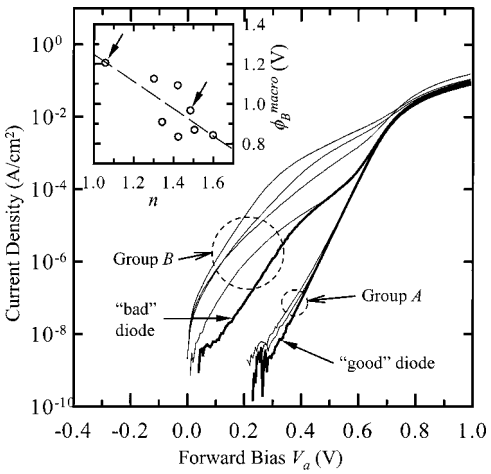

FIG. 1. Measured diode *I-V* curves of a set of Pd/6*H*-SiC contacts, which appear to be divided into group A (relatively ideal behavior) and group B (highly nonideal). Thick curves marked by arrows indicate a particular ''good'' and a ''bad'' diode chosen for detailed analysis (see text). The good diode shows macroscopic SBH $\phi_B^{\mathrm{macro}}\cong1.21$ V and ideality factor $n\cong1.06$, whereas the bad diode has $\phi_B^{\mathrm{macro}}\cong0.97$ V and $n\cong1.49$. Inset: measured ϕ_B^{macro} versus *n* for the different diodes. Arrows mark the two chosen diodes.

Ohmic to highly rectifying. Figure 1 plots forward-bias diode *I-V* curves of several of the rectifying diodes. Substantial device-to-device variation is obvious, even though the diodes were prepared under nominally identical conditions. For each rectifying diode, the ''macroscopic'' SBH (ϕ_B^{macro}),[21] ideality factor (*n*), and series resistance (R_s) were extracted by fitting the thermionic emission equation (for $V_a>3k_BT/q$)[2,22]

$$I=AA^*T^2\exp(-q\phi_B^{\mathrm{macro}}/k_BT)\times\{\exp[q(V_a-R_sI)/nk_BT]-1\} \quad (1)$$

to a portion of the measured *I-V* curves that appears approximately linear on a semilog plot (the abscissa being V_a). Here, V_a is the applied external bias, *A* is device area ($\cong1.96\times10^{-3}\,\mathrm{cm}^2$), A^* is the 6*H*-SiC Richardson constant ($\cong156\ \mathrm{A\,cm^{-2}\,K^{-2}}$), *q* is the electronic charge, k_B is the Boltzmann constant, and *T* is the sample temperature ($\cong294$ K). Note that the actual voltage drop *V* across the depletion region is $V=V_a-R_sI$. The inset of Fig. 1 plots ϕ_B^{macro} versus *n*, showing a pronounced correlation between the two parameters. This correlation is similar to that reported by other authors,[12,19,23] who also proposed that a ''homogeneous'' or ''zero bias'' barrier height ϕ_B^{hom}, could be deduced by extrapolating the plot back to $n=n_{if}\approx1.01$.[24] In our case, a least-squares fit of the data (the dashed line in the inset of Fig. 1) gives $\phi_B^{\mathrm{hom}}\cong1.24\pm0.09$ V.

From Fig. 1, we see that the different diodes can be roughly divided into two groups, those with roughly ideal behavior down to low forward bias (group A) and those with significant nonidealities below ~0.6 V forward bias (group B). In order to compare the macroscopic and nm-scale behavior in more detail, two devices were chosen as examples for nm-scale analysis, which we refer to as a ''good'' and a

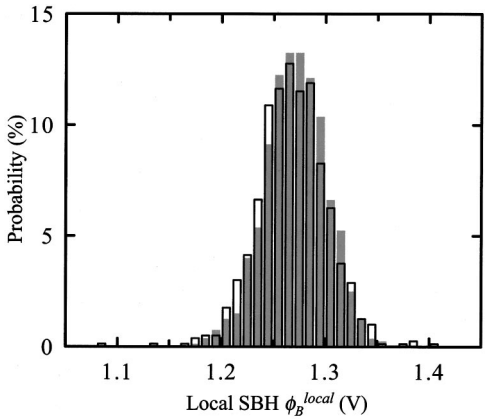

FIG. 2. Measured nm-scale barrier height distributions of the good diode (gray solid bars) and the bad diode (empty bars) as determined by fitting 800 BEEM spectra using the Bell-Kaiser theory (see text). The estimated fitting error due to system noise is $\sigma_{\text{noise}} \cong 0.02$ V. The two distributions are identical within statistical uncertainties.

''bad'' diode, respectively. The *I-V* curves of these two diodes are plotted with thicker lines and marked by the appropriate arrows in Fig. 1. The good diode shows very ideal diode behavior over a wide voltage range (with $\phi_B^{\text{macro}} \cong 1.21$ V and $n \cong 1.06$), whereas the bad diode shows severely nonideal behavior ($\phi_B^{\text{macro}} \cong 0.97$ V and $n \cong 1.49$ over a fitting range from 0.12 to 0.38 V). The nm-scale BHD for both diodes was measured using BEEM,[18] a technique based on scanning tunneling microscopy that can measure (among other things) the local barrier height at Schottky interfaces with a nm-scale resolution.[14,17,25–27] Both diodes had sufficiently high zero bias resistance (>55 and 8 GΩ for the good and bad diodes, respectively) so that BEEM measurement could be made with a high signal-to-noise ratio. Diodes with much smaller zero bias resistance have larger background noise in the measured BEEM current, due to larger thermal noise and increased susceptibility to external voltage fluctuations.

On each of the good and bad diodes, 800 BEEM spectra were taken at different locations over the sample surface, each separated by at least 30 nm. Each BEEM spectrum was fit using the Bell-Kaiser model[18] to extract the local SBH ϕ_B^{local}. Figure 2 shows the measured distributions of ϕ_B^{local} of the two diodes. (Notice that the histograms are interpreted as the BHDs.) The good diode had a measured mean SBH $\langle \phi_B^{\text{local}} \rangle_{\text{good}} = 1.271$ V and standard deviation $\sigma_{\text{meas}} = 29$ mV, while for the bad diode $\langle \phi_B^{\text{local}} \rangle_{\text{bad}} = 1.268$ V and $\sigma_{\text{meas}} = 33$ mV. The experimental uncertainty in the extracted ϕ_B^{local} from each BEEM spectrum is estimated[28] to be $\sigma_{\text{noise}} \cong 20$ mV, which is due mostly to ~35 fA of noise in the measured BEEM current. Here we note two things: (1) The measured BHDs of the good and bad diodes are essentially identical, within statistical fluctuations. This gives immediate and strong evidence that nonidealities in the bad diode are probably due to a small pathological fraction of the sample area that was not sampled by BEEM. We will return to this point later. (2) Since the experimental uncertainty is of comparable magnitude as the measured spread in the BHD, we conclude that the *actual* variations in barrier height are to be reduced from the measured distributions approximately as $\sigma_{\text{actual}} \approx \sqrt{\sigma_{\text{meas}}^2 - \sigma_{\text{noise}}^2} \cong 21$ or 26 mV, for the good and bad diode, respectively. This represents the *largest* spread that the actual BHD could reasonably have without contradicting the measured BHDs shown in Fig. 2. For the subsequent analysis, we take $\sigma_{\text{limit}} \approx 30$ mV as a conservative *upper limit* for the spread in the actual BHD.

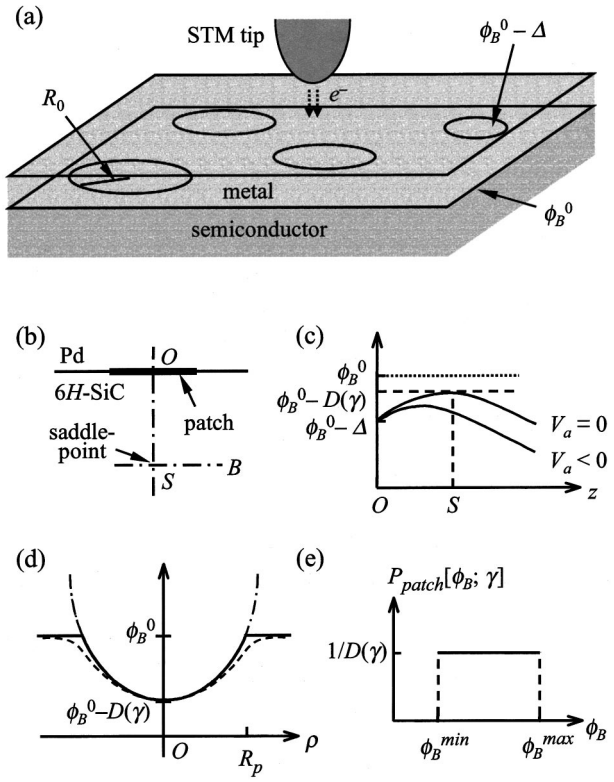

FIG. 3. (a) Schematic of the Tung model. A random distribution of circular patches of size R_0 and barrier height $\phi_B^0 - \Delta$ in the otherwise homogeneous background of SBH ϕ_B^0. (b) A patch of size comparable to or smaller than the semiconductor Debye length gives rise to a potential saddle-point *S* beneath the patch center *O*. (c) Potential profile along the interface normal (along *O*-*S*) for zero applied bias V_a, and for a reverse bias ($V_a < 0$). Reverse bias reduces the potential maximum (i.e., an *increased depth*) near *S*. (d) Lateral profile of the potential maximum projected normally onto the MS interface. The dashed line is the exact potential, the dash-dot line is Tung's parabolic approximation, and the solid line is the truncated paraboloid used to calculate the microscopic BHD. (e) Calculated probability density for a single low-barrier patch of strength γ, with $\phi_B^{\min} = \phi_B^0 - D(\gamma)$ and $\phi_B^{\max} = \phi_B^0$.

B. The Tung model and calculated diode *I-V* curve

The Tung model[8] envisioned an areal density[29] c_1 of circular ''patches'' having varying interfacial barrier height embedded in uniform background of barrier height ϕ_B^0 [see Fig. 3(a)]. An individual patch was assumed to have a radius R_0 and a potential depth Δ relative to the background barrier height. Tung pointed out that a patch could (in certain limits)

be treated approximately as an electrostatic *dipole* moment p of strength $p=2\epsilon_s\Delta\pi R_0^2$, where ϵ_s is the permittivity of the semiconductor. Instead of directly dealing with individual distributions of Δ and R_0, Tung defined a ''patch parameter'' $\gamma\equiv 3(R_0^2\Delta/4)^{1/3}=(27/8\pi\epsilon_s)^{1/3}p^{1/3}$ and analyzed models in which γ was assumed to have a particular distribution, such as a delta-function distribution or a Gaussian distribution with a width σ_γ.[8] Most subsequent analysis has focused on an assumed Gaussian distribution of γ given by a probability density function $P[\gamma]=e^{-\gamma^2/2\sigma_\gamma^2}/\sqrt{2\pi\sigma_\gamma^2}$,[29] since it is expected that a range of nonideal patches could be present in a real physical system.[9,11,12,15] Tung assumed that both higher-barrier and lower-barrier patches could be present in the real system, but neglected the high-barrier patches in his calculation of excess (thermionic) diode current, since this excess current would fall off exponentially with barrier height and the patches were assumed to cover a relatively small fraction of the entire diode area. However, our BEEM measurements probe the local barrier height directly, and hence would be just as sensitive to high-barrier patches as low barrier ones. So for the calculated BHD (see next sections), we include both low-barrier patches (with $\gamma>0$) and high-barrier patches (with $\gamma<0$).

Tung pointed out that the local barrier height variation around a lower-barrier dipole patch is characterized by a ''potential pinch-off'' condition, with a corresponding *saddle-point* barrier height variation [point *S* in Fig. 3(b)]. In the direction normal to the interface [line *O*-*S* in Fig. 3(b)], this potential profile has a *maximum* at this saddle point [see Fig. 3(c)], located at some depth in the semiconductor directly behind the patch. However, the potential has a *minimum* at the saddle point along a line parallel to the interface [line *S*-*B* in Fig. 3(b)]. This is illustrated in Fig. 3(d). The dashed line in the figure represents the lateral profile of the potential maximum projected normally onto the MS interface. The maximum depth $D(\gamma)$ of this potential (relative to the background ϕ_B^0) is given by[8] $D(\gamma)=\gamma(V_{bb}/\eta)^{1/3}$, where $V_{bb}=\phi_B^0-(E_C-E_F)_{\text{neutral}}-V$ is the band bending of the MS junction, $(E_C-E_F)_{\text{neutral}}$ is the depth of Fermi level relative to the conduction band minimum deep in the semiconductor bulk,[30] and $\eta\equiv\epsilon_s/qN_D$. To simplify the calculations, Tung approximated this potential cross section by a paraboloid (a cylindrically symmetric second-order expansion), schematically shown by the dash-dotted line in Fig. 3(d) and given explicitly by the expression

$$V(\rho,z_{\text{saddle}})\cong\phi_B^0-D(\gamma)+\frac{9}{\gamma}\left(\frac{V_{bb}}{2W}\right)^{4/3}\rho^2, \tag{2}$$

where the saddle point *S* is denoted by $(\rho,z)=(0,z_{\text{saddle}})$.

Tung then calculated the excess diode current from a patch by integrating the thermionic emission current equation over this parabolic potential profile. Tung's calculated current for a single patch is[8]

$$I_{\text{patch}}(\gamma)=A^*T^2(4\pi\gamma\eta^{2/3}/9\beta V_{bb}^{2/3})\exp\{-\beta[\phi_B^0-D(\gamma)]\}\times[\exp(\beta V)-1], \tag{3}$$

where $\beta\equiv q/k_BT$. The second-order expansion of the potential is quite accurate close to the potential minimum, but becomes inaccurate and greatly exceeds the background potential ϕ_B^0 far away from the potential minimum. This does not significantly affect the calculated thermionic current (which falls off exponentially at higher potential), but would introduce unphysically large barrier heights in the calculated BHD. For the calculated BHD (see next section), we therefore *truncate* the second order expansion of the potential at a radius $R_{\text{patch}}(\gamma)=(\frac{1}{3})(2W/V_{bb})^{2/3}\sqrt{\gamma D(\gamma)}$, where it is equal to ϕ_B^0. This is shown by the solid curve in Fig. 3(d)). Here $W=(2\epsilon_sV_{bb}/qN_D)^{1/2}$ is the semiconductor depletion width. Note that $R_{\text{patch}}(\gamma)$ is not directly related to R_0 defined previously. We also define an effective area[29] of an individual patch as $A_{\text{patch}}(\gamma)\equiv\pi[R_{\text{patch}}(\gamma)]^2$ and the fractional coverage of all the patches as $C_p\equiv\Sigma_\gamma A_{\text{patch}}(\gamma)/A$, where the summation is over the assumed patch distribution. For the case of a Gaussian patch distribution of width σ_γ, this reduces to $C_p=\pi c_1\sigma_\gamma^2(16W^4/\eta)^{1/3}/9V_{bb}$. Note that $D(\gamma)$, $R_{\text{patch}}(\gamma)$, $A_{\text{patch}}(\gamma)$, and C_p all depend implicitly on the applied bias V_a through the band-bending term V_{bb}. Tung then calculated the net diode current by integrating Eq. (3) over the assumed distribution of patches, and adding the current from the uniform background. This total current can be expressed by

$$I_{\text{total}}=c_1A\int_0^\infty P[\gamma]I_{\text{patch}}(\gamma)d\gamma+I_{\text{background}} \tag{4a}$$

$$=AA^*T^2\exp(-\beta\phi_B^0)[\exp(\beta V_a)-1]\times\{1-C_p+(2\pi c_1\sigma_\gamma^2\eta^{1/3}/9V_{bb}^{1/3})\times\exp(\beta^2\sigma_\gamma^2V_{bb}^{2/3}/2\eta^{2/3})[1+\text{erf}(\beta\sigma_\gamma V_{bb}^{1/3}/\sqrt{2}\,\eta^{1/3})]\}, \tag{4b}$$

where erf stands for the error function. Equation (4b) is essentially identical to that derived by Tung, except that we have explicitly reduced the contribution of $I_{\text{background}}$ by a factor of $(1-C_p)$ to account for the fraction of the diode area covered by the patches.

C. nm-scale BHD calculated from the Tung model

We next use the Tung model to calculate the expected BHD for a particular patch-parameter distribution, so that it can be compared with the measured BHDs shown in Fig. 2. We first consider the expected BHD for a diode with zero applied bias ($V_a=0$), since the data in Fig. 2 was measured at $V_a=0$. We proceed by first considering the BHD of an individual patch of strength γ, then averaging over a Gaussian patch-parameter distribution, and then including the uniform background distribution. It is straightforward to calculate the BHD for an individual patch, since the potential around a patch is assumed to be a truncated paraboloid as shown in Fig. 3(d). The BHD $P_{\text{patch}}[\phi_B;\gamma]$ for an individual paraboloid turns out to be a *uniform* distribution, as shown in Fig. 3(e). This uniform distribution is bounded from $\phi_B^{\min}=\phi_B^0-D(\gamma)$, corresponding to locations directly over the cen-

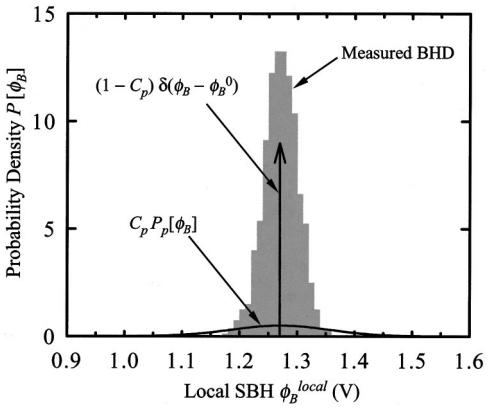

FIG. 4. Solid lines: calculated BHD $P_{\rm model}[\phi_B]$ from the Tung model, consisting of a Dirac δ function (arrow) from the uniform background and a Gaussian distribution for the patches, using parameter values from the solid curve in Fig. 5 (see text). Gray bars: measured BHD of the good diode from Fig. 2.

ter of the patch, to $\phi_B^{\max}=\phi_B^0$ at the edge of the patch, and has an amplitude $[D(\gamma)]^{-1}$ to ensure that $P_{\rm patch}[\phi_B;\gamma]$ is properly normalized. Patches with barrier heights higher than ϕ_B^0 are assumed to contribute to $P_{\rm patch}[\phi_B;\gamma]$ in a symmetric way with $\phi_B^{\min}=\phi_B^0$ and $\phi_B^{\max}=\phi_B^0-D(\gamma)$, where both γ and $D(\gamma)$ are taken to be negative for high-barrier patches. We note that this actually underestimates the contribution from high-barrier patches, since potential pinch-off occurs only for low-barrier patches.[8] A more accurate calculation can only be made if one knows the *separate* distributions for the radius R_0 and a potential depth Δ of the high-barrier patches, but which are only included *jointly* as the patch strength γ in the Tung model. However, since this *underestimates* the spread in the BHD, we can still use these calculations to determine what range of parameter values would produce a nm-scale BHD that *exceeds* the measured BHD. This is discussed in more detail later in this section.

We next calculate the BHD $P_p[\phi_B]$ for all the patches, but not yet including the uniform background regions. This is given by

$$P_p[\phi_B]=\frac{\Sigma_\gamma A_{\rm patch}(\gamma)P_{\rm patch}[\phi_B;\gamma]}{\Sigma_\gamma A_{\rm patch}(\gamma)}. \tag{5}$$

The patch area $A_{\rm patch}(\gamma)$ is included because the probability that the probe tip lands over a particular patch is proportional to the patch area. Since the distribution in γ is assumed to be Gaussian, it turns out that $P_p[\phi_B]$ is itself a Gaussian function[31] of ϕ_B, centered at ϕ_B^0 with a width $\sigma_p=(V_{bb}/\eta)^{1/3}\sigma_\gamma$.

Finally, we can write an expression for the model BHD of the *entire* diode:

$$P_{\rm model}[\phi_B]=C_pP_p[\phi_B]+(1-C_p)\,\delta(\phi_B-\phi_B^0). \tag{6}$$

The first term is due to all the patches (which cover a fraction C_p of the total diode area), while the δ function in the second term describes the uniform background. Figure 4 shows an example of what $P_{\rm model}[\phi_B]$ should look like, assuming $\phi_B^0=1.271$ V, $c_1=6.0\times10^9\,{\rm cm}^{-2}$, and $\sigma_\gamma=1.03\times10^{-4}\,{\rm V}^{1/3}\,{\rm cm}^{2/3}$. This model distribution consists of a sharp, delta-function central peak (due to the uniform background areas of the diode) superimposed on a broad ''wing'' (due to the patches) of width σ_p and integrated probability $C_p=0.107$. Once we have the model BHD as given by Eq. (6), it is easy to calculate the overall standard deviation of this model distribution

$$\sigma_{\rm model}=\sqrt{C_p}\,\sigma_p=\sqrt{C_p}(V_{bb}/\eta)^{1/3}\sigma_\gamma. \tag{7}$$

The Tung model is essentially defined by three parameters: the background barrier height ϕ_B^0, the number density of patches c_1, and the width σ_γ of the Gaussian patch-parameter distribution. These three parameters determine both the expected macroscopic diode I-V characteristic [Eq. (4)] and the expected nm-scale BHD [Eq. (6)]. In principle, it seems we should be able to extract all three parameters directly from the measured BHD. The mean value of the measured BHD would give us ϕ_B^0, and the width and total area of the wing part of the distribution would give us σ_p and C_p, which in turn could be used to extract the intrinsic model parameters c_1 and σ_γ. However, a comparison of the model BHD and the measured BHD (see Fig. 4) shows that this is not directly possible. The problem is that the measured BHD does not have a distinct (resolvable) sharp central peak and a distinct wing region. This makes it difficult to decide how much of the measured BHD is due to the patches (the wing), and how much is part of the uniform background (the sharp peak). There are several reasons for this. First, the measurement uncertainty ($\sigma_{\rm noise}\cong20$ mV) is comparable to the measured width of the BHD ($\sigma_{\rm meas}\cong30$ mV), and hence would significantly broaden any sharp central peak. Second, the Tung model itself is at best an approximate description of the true interface. In particular, the ''uniform background'' of a real MS system is *probably not perfectly uniform*, and likely has some variation in barrier height that would broaden the central peak. Third, the experimental statistics at the edges of the measured BHD are not very high, making it difficult to clearly identify and quantify a ''wing'' distribution due to patches. Nevertheless, it is important to realize that the measured BHD can still be used to test the parameter values assumed for the Tung model as applied to a particular Schottky diode. In particular, we can rule out parameter values that would result in $\sigma_{\rm model}>\sigma_{\rm limit}\cong30$ mV, since the measured BHD (Fig. 2) is not consistent with a model distribution wider than $\sigma_{\rm limit}$.

In order to compare the measured and model behaviors, we accordingly adopt the following procedure. (1) The parameter ϕ_B^0 is determined directly from the *mean* of the measured BHD from a particular diode: $\phi_B^0=\langle\phi_B^{\rm local}\rangle$. (2) We assume a particular value of the patch density c_1, which is treated as a free parameter. (3) The parameter σ_γ is then determined so the calculated macroscopic diode I-V characteristic [Eq. (4)] will be consistent with the measured I-V characteristic for that diode. (4) This set of parameters implies a particular value of $\sigma_{\rm model}$ for the nm-scale BHD. This is compared with the measured upper limit $\sigma_{\rm limit}\cong30$ mV. If $\sigma_{\rm model}>\sigma_{\rm limit}$, then we reject this particular set of parameters, since it would result in a broader distribution of nm-

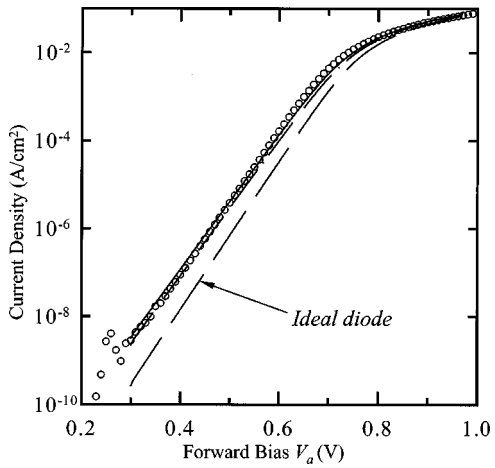

FIG. 5. Comparison of calculated (lines) and measured (empty circles) diode I-V's for the good diode. All the curves assume $\phi_B^0 = \langle \phi_B^{\text{local}} \rangle_{\text{good}} = 1.271\,\text{V}$. Dashed line: ideal I-$V(c_1=0)$ with $n = n_{if}$ (Ref. 24). Dash-dot line: $c_1 = 3.0\times10^9\,\text{cm}^{-2}$ and $\sigma_\gamma = 1.06\times10^{-4}\,\text{V}^{1/3}\,\text{cm}^{2/3}$. Solid line: $c_1 = 6.0\times10^9\,\text{cm}^{-2}$, and $\sigma_\gamma = 1.03\times10^{-4}\,\text{V}^{1/3}\,\text{cm}^{2/3}$.

scale barrier heights than are actually measured. Finally, we try different values of the patch density c_1, to see what range of parameter values is consistent with measurements for a particular diode.

D. Case study: The ''good'' diode

We first do this comparison for the ''good'' diode shown in Fig. 1. We start by considering the case of an *ideal diode*, for which the patch density $c_1 = 0$. As discussed above, the parameter ϕ_B^0 is directly determined by the mean of the measured BHD, which for the good diode gives $\phi_B^0 = \langle \phi_B^{\text{local}} \rangle_{\text{good}} = 1.271\,\text{V}$. Using this parameter in the ideal diode equation [Eq. (1), with ideality factor[24] $n = n_{if}$], we get the long-dashed line shown in Fig. 5. We see that this ideal curve fits the measured data (empty circles) well at high bias, but deviates somewhat at lower bias. Much better agreement with measurement can be found using the Tung model for a particular range of parameter values. For example, the dash-dot line in Fig. 5 was calculated using Eq. (4) with the parameters $\phi_B^0 = \langle \phi_B^{\text{local}} \rangle_{\text{good}} = 1.271\,\text{V}$,[32] patch density $c_1 = 3.0\times10^9\,\text{cm}^{-2}$, and $\sigma_\gamma = 1.06\times10^{-4}\,\text{V}^{1/3}\,\text{cm}^{2/3}$, while the solid line in Fig. 5 was calculated using $\phi_B^0 = 1.271\,\text{V}$, $c_1 = 6.0\times10^9\,\text{cm}^{-2}$, and $\sigma_\gamma = 1.03\times10^{-4}\,\text{V}^{1/3}\,\text{cm}^{2/3}$. These two parameter sets imply fractional patch coverage $C_p \cong 5.7$ and 10.7 %, respectively. As discussed above, it is important to check that a particular set of parameters is consistent with the measured nm-scale BHD. It turns out that these two parameter sets imply $\sigma_{\text{model}} = 21$ and 28 mV, respectively, so both parameter sets are consistent with the measured upper limit $\sigma_{\text{limit}} \approx 30\,\text{mV}$. Therefore, the Tung model with these parameter values is consistent with both the macroscopic diode I-V curve, as well as the nm-scale BHD. We find that only parameter sets with c_1 in the range of 3×10^9 to $1\times10^{10}\,\text{cm}^{-2}$ and corresponding σ_γ in the range of 0.94×10^{-4} to $1.06\times10^{-4}\,\text{V}^{1/3}\,\text{cm}^{2/3}$ are consistent with both the macroscopic I-V data as well as the nm-scale BHD. In a later section, we discuss how the measured BHD varies with applied diode bias V_a, and show that this behavior also is consistent with the Tung model for parameter sets in this range.

E. Case study: The ''bad'' diode

As can be seen from Fig. 1, the ''bad'' diode exhibits substantially more current at small forward bias than either the ''good'' diode, or the expected ideal behavior. As a figure of merit, we note that the bad diode exhibits about 4000 times as much current at 0.3 V forward bias than the ideal behavior. We now consider what range of parameter values in the Tung model could result in this range of excess current at 0.3 V forward bias, and then check to see if these parameters are consistent with the measured BHD of the bad diode. The parameter $\phi_B^0 = \langle \phi_B^{\text{local}} \rangle_{\text{bad}} = 1.268\,\text{V}$ is determined directly from the mean of the measured BHD. We then consider different possible values of c_1 (listed in the first column of Table I), determine the corresponding value of σ_γ that would give 4000 times excess current at 0.3 V (shown in the second column in Table I), calculate the resulting σ_{model} (third column), which then can be compared with the measured upper limit of $\sigma_{\text{limit}} \approx 30\,\text{mV}$. The fourth and fifth columns of Table I show fractional patch coverage and the potential depth of a typical patch (i.e., a patch of strength σ_γ), respectively. The other columns will be discussed later.

TABLE I. For a range of patch density c_1, σ_γ is optimized to produce measured diode current at $V_a = 0.3\,\text{V}$ for the bad diode. From c_1 and σ_γ, the BHD width $\sigma_{\text{model}}[\phi_B]$, the patch coverage C_p, the typical patch depth $D(\sigma_\gamma)$, and the dominant patch depth $D(\gamma_d)$ are calculated at $V_a = 0\,\text{V}$. The dominant patch parameter γ_d is evaluated at $V_a = 0.3\,\text{V}$.

c_1 (cm^{-2})	σ_γ ($\text{V}^{1/3}\,\text{cm}^{2/3}$)	$\sigma_{\text{model}}[\phi_B]$ (V)	C_p (%)	$D(\sigma_\gamma)$ (V)	γ_d/σ_γ	$D(\gamma_d)$ (V)	N_{tail}
1×10^{10}	1.47×10^{-4}	0.074	36.6	0.122	4.51	0.55	62.2
3×10^{9}	1.56×10^{-4}	0.045	12.3	0.129	4.75	0.61	5.94
1×10^{9}	1.63×10^{-4}	0.029	4.49	0.135	4.96	0.67	0.69
3×10^{8}	1.71×10^{-4}	0.017	1.48	0.142	5.18	0.73	0.066
1×10^{8}	1.78×10^{-4}	0.011	0.53	0.147	5.37	0.79	7.6×10^{-3}
3×10^{7}	1.85×10^{-4}	0.006	0.17	0.153	5.58	0.86	7.1×10^{-4}
1×10^{7}	1.92×10^{-4}	0.004	0.06	0.159	5.76	0.92	8.2×10^{5}

Table I indicates that in the high-coverage limit ($c_1 > 1 \times 10^9\,\mathrm{cm}^{-2}$), the resulting value of σ_{model} is larger than $\sigma_{\mathrm{limit}} \approx 30\,\mathrm{mV}$. This means that we can reject parameter sets that include $c_1 > 1 \times 10^9\,\mathrm{cm}^{-2}$, since they would result in a nm-scale BHD that is larger than what is actually measured. Hence, the only way that the Tung model (with a Gaussian patch distribution) could account for the observed nonideal I-V behavior of the ''bad'' diode and still be consistent with the measured BHD, is if the patch density $c_1 < 1 \times 10^9\,\mathrm{cm}^{-2}$. We see from Table I that this corresponds to a fractional patch coverage $C_p < \sim 5\%$. Note that at these smaller patch densities c_1, the patches must be *deeper* (on average) to give the required excess current. But the required patch depth increases only weakly with decreasing c_1 (as shown in the fifth column of Table I) since the excess current depends exponentially on patch depth. Consequently, σ_{model} decreases strongly with the patch density c_1. Another way to think about this is that it becomes progressively less probable for the probe tip to land over a patch in the low-coverage limit, and hence the patches contribute progressively less to the overall BHD measured by BEEM.

Although we cannot directly rule out the range of patch distributions with $c_1 < 1 \times 10^9\,\mathrm{cm}^{-2}$, a more detailed analysis of the Tung model reveals something surprising. It turns out that most of the excess current would be contributed by an extremely small number of particularly deep patches in the extreme tail of the Gaussian patch distribution. The number of such ''dominant'' patches becomes so small for $c_1 < 1 \times 10^9\,\mathrm{cm}^{-2}$, that one would expect (on average) fewer than one such dominant patch in a typical diode structure. To see this, we examine Eq. (4a) in more detail to determine what range of γ gives the largest contribution to the excess current. The patch density falls off sharply with γ [since $P[\gamma] \propto \exp(-\gamma^2/2\sigma_\gamma^2)$], but the thermionic current though a patch increases strongly with γ (since $I_{\mathrm{patch}}(\gamma) \propto \gamma \exp[\beta D(\gamma)]$; see Eq. (3)). Consequently, the integrand in Eq. (4a) is peaked at a value of $\gamma = \gamma_d$, where

$$\gamma_d = \frac{1}{2}\sigma_\gamma^2 \beta \left(\frac{V_{bb}}{\eta}\right)^{1/3} \left(1 + \sqrt{1 + \frac{4}{\sigma_\gamma^2 \beta^2}\left(\frac{\eta}{V_{bb}}\right)^{2/3}}\right). \quad (8)$$

It turns out that γ_d is surprisingly deep for 6H-SiC (as shown in the sixth column of Table I) and falls far into the tail of the assumed Gaussian distribution of γ. We note three important points about these dominant patches. First, roughly half the excess diode current is due to patches with $\gamma > \gamma_d$. Secondly, the corresponding depth of these dominant patches below ϕ_B^0 is very large (as shown in the seventh column of Table I), and is deeper than ~ 0.7 V for $c_1 < 1 \times 10^9\,\mathrm{cm}^{-2}$. And, finally, the actual number of the dominant patches (with $\gamma > \gamma_d$) in a typical (0.5-mm-diameter) diode is extremely small. As a figure of merit we define $N_{\mathrm{tail}} \equiv c_1 A \int_{\gamma_d}^{\infty} P[\gamma] d\gamma$, which is shown in the last column of Table I. We see that N_{tail} is very small (<1) for $c_1 < 1 \times 10^9\,\mathrm{cm}^{-2}$, and is extremely small (<0.01) for $c_1 < 1 \times 10^8\,\mathrm{cm}^{-2}$. Hence even if a set of diodes were prepared to be nominally identical (i.e., with identical parameter values), one would still expect extremely large *statistical* fluctuations in the number of deep patches present in different diodes, with corresponding large fluctuations in the excess current.

Hence, the Tung model in the limit of $c_1 < 1 \times 10^9\,\mathrm{cm}^{-2}$ appears to be somewhat similar to the view of nonideal I-V behavior observed in metal/4H-SiC Schottky diodes proposed by Skromme *et al.*,[19] who argued that the excess current was correlated with a very small number of gross (μm-sized) *deep* defects visible by electron beam induced current (EBIC) imaging. However, Skromme *et al.* suggested that these defects were essentially of *extrinsic* origin, i.e., due to crystal defects (such as screw dislocations, epilayer pits, stacking faults, and polytype inclusions) or localized contamination introduced during diode preparation. In contrast, the Tung model outlined above would ascribe such deep defects to the extreme tail of an otherwise broad, essentially *intrinsic* patch distribution.

Which view is more correct for the metal SiC system? We believe that a combination of these two views actually makes the most sense. We propose that *most* of the surface area of *both* the good and the bad diodes should be well characterized by a Tung model with a large coverage of shallow patches (e.g., with parameters $c_1 \approx 5 \times 10^9\,\mathrm{cm}^{-2}$, and $\sigma_\gamma \approx 1 \times 10^{-4}\,\mathrm{V}^{1/3}\,\mathrm{cm}^{2/3}$), but the bad diodes also contain a few gross defects of extrinsic origin, which dominate the excess current observed at low bias. This would explain in a natural way (1) the excellent agreement for the good diode to the Tung model with respect to *both* the macroscopic I-V curves (Fig. 5) and the nm-scale BHD (Fig. 2), (2) the nearly identical measured BHDs for the good and bad diodes (Fig. 2), and (3) the observed ''grouping'' of the diodes (see Fig. 1), where group A in Fig. 1 presumably contains diodes with no gross extrinsic defects, while group B contains diodes with one or more extrinsic defects.

F. Effect of reverse bias on the nm-scale BHD

We have proposed that most of the surface area of all the diodes is well characterized by a Tung model with a significant coverage of shallow patches. If this is true, then there should be an additional, observable effect: the BHD measured by BEEM should actually *become broader* if a reverse bias is applied across the diode during BEEM measurement. This is because the depth below background of a particular patch *increases* with increasing reverse bias, as illustrated in Fig. 3(c). This should result in an increase in the distribution of local barrier heights. We investigated this effect for the good diode, by measuring sets of 100 BEEM spectra to sample the BHD at a particular reverse bias, determining the spread σ_{meas} in this sampled BHD, and plotting σ_{meas} as a function of the applied reverse bias. The results of these measurements are shown in Fig. 6. We have included in Fig. 6 a data point determined from the BHD shown in Fig. 2, which was measured at $V_a = 0$. Although the data points have significant fluctuations, we do in fact observe a general *increase* in σ_{meas} with increasing reverse bias. Since a small current will flow through the diode under reverse bias, one should be concerned that this might introduce extra current noise into the BEEM measurements, which could increase the uncertainty σ_{noise} in the measured local barrier height.

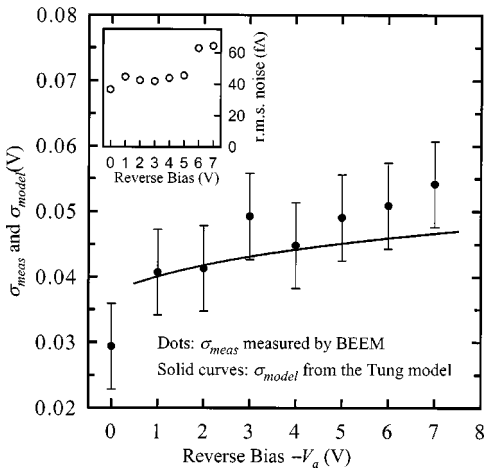

FIG. 6. Data points: Width σ_{meas} of measured BHD variation vs reverse bias $-V_a$. Solid curve: Calculated BHD width $\sigma_{\mathrm{model}}[\phi_B]$ assuming $c_1 = 6.0\times 10^9\,\mathrm{cm}^{-2}$, and $\sigma_\gamma = 1.03\times 10^{-4}\,\mathrm{V}^{1/3}\,\mathrm{cm}^{2/3}$, and $\sigma_{\mathrm{noise}} \cong 25\,\mathrm{mV}$. Inset: Root-mean-squared current noise of BEEM signal versus applied reverse bias.

The inset of Fig. 6 shows the measured current noise level as a function of reverse bias. We see that the average current noise is ~20% higher for the reverse bias of 1 V or larger, and accordingly we estimate the system noise under reverse bias to be about $\sigma_{\mathrm{noise}} \cong 25\,\mathrm{mV}$, as compared to our earlier estimate of $\sigma_{\mathrm{noise}} \cong 20\,\mathrm{mV}$ at zero applied bias. However, the inset also shows that the current noise remains relatively constant at least up to $-V_a = 5$ V. We therefore believe the observed increase in σ_{meas} with $-V_a$ represents an increase in the actual BHD, and is not simply due to increased system noise. Interestingly the current noise shows a sharp increase at $-V_a = 6$ V, which may be partly responsible for the larger deviation of σ_{meas} from the model calculation (see below) at $-V_a = 6$ and 7 V.

As discussed in Sec. III C, the expected ''true'' width of the BHD from the Tung model is given by Eq. (7), where V_{bb} and C_p both depend implicitly on the applied bias. To compare with the observed values of σ_{meas} shown in Fig. 6, we need to broaden σ_{model} by the system noise as $\sigma_{\mathrm{model}} = \sqrt{C_p \sigma_\gamma^2 (V_{bb}/\eta)^{2/3} + \sigma_{\mathrm{noise}}^2}$. This is shown by the solid line in Fig. 6, where we have assumed parameter values $\phi_B^0 = 1.271$ V, $c_1 = 6.0\times 10^9\,\mathrm{cm}^{-2}$, and $\sigma_\gamma = 1.03 \times 10^{-4}\,\mathrm{V}^{1/3}\,\mathrm{cm}^{2/3}$. We see that the expected increase in σ_{model} with increasing reverse bias agrees reasonably well with the observed increase, giving further support to the proposal that the good diode is well characterized by a Tung model with these particular parameter values.

IV. CONCLUSIONS

We have used the Tung model[8] to calculate the expected nm-scale barrier-height distribution (BHD) for particular parameter values, measured the nm-scale BHD of particular Schottky diodes using UHV BEEM, and directly related the measured nm-scale BHD of a particular Schottky diode to its macroscopic I-V characteristic. Our results indicate that (1) for a relatively ideal 6H-SiC diode, the Tung model with high coverage of shallow patches describe very well both the macroscopic and nm-scale behaviors, while (2) the Gaussian Tung model could account for more nonideal diodes only by assuming an extremely different patch-parameter distribution which is dominated by a few patches in the extreme tail of the distribution. We instead propose that most of the surface area of all the diodes consists of a broad distribution of many shallow patches, while significantly nonideal diodes also contain a few gross defects of extrinsic origin[19] that dominate the nonideal behavior at low bias. The proposed model would explain the measured nm-scale BHDs and macroscopic I-V characteristics of both the ''good'' and ''bad'' diodes, the observed increase in the measured BHD at reverse diode bias, and the observed large diode-to-diode variations and ''grouping'' of the macroscopic I-V characteristics.

ACKNOWLEDGMENTS

The authors thank O. Shigiltchoff, R. P. Devaty, and E. R. Heller for helpful comments and suggestions. The work done at the Ohio State University was supported by the Office of Naval Research under Grant No. N00014-93-1-0607.

*Electronic mail: hjim@mps.ohio-state.edu

[1] L. J. Brillson, Surf. Sci. Rep. **2**, 123 (1982); R. T. Tung, J. Vac. Sci. Technol. B **11**, 1546 (1993).
[2] E. H. Rhoderick and R. H. Williams, *Metal-Semiconductor Contacts*, 2nd ed. (Oxford University Press, Oxford, 1988).
[3] *Silicon Carbide: A Review of Fundamental Questions and Applications to Current Device Technology*, edited by W. J. Choyke, H. Matsunami, and G. Pensl (Akademie Verlag, GmbH, Berlin, 1997).
[4] *Silicon Carbide, III-Nitrides and Related Materials*, edited by G. Pensl, H. Morkoç, B. Monemar, and E. Janzén (Trans Tech publications, Switzerland, 1998).
[5] J. L. Freeouf, T. N. Jackson, S. E. Laux, and J. M. Woodall, Appl. Phys. Lett. **40**, 634 (1982).
[6] I. Ohdomari and H. Aochi, Phys. Rev. B **35**, 682 (1987).
[7] A. I. Bastys, V. B. Bikbaev, J. J. Vaitkus, and S. C. Karpinskas, Litov. Fiz. Sb. **28**, 191 (1988).
[8] R. T. Tung, Phys. Rev. B **45**, 13 509 (1992); Appl. Phys. Lett. **58**, 2821 (1991).
[9] H. H. Weitering, J. P. Sullivan, R. J. Carolissen, R. Pérez-Sandoz, W. R. Graham, and R. T. Tung, J. Appl. Phys. **79**, 7820 (1996).
[10] S. Anand, S-B. Carlsson, K. Deppert, L. Montelius, and L. Samuelson, J. Vac. Sci. Technol. B **14**, 2794 (1996).
[11] A. Olbrich, J. Vancea, F. Kreupl, and H. Hoffmann, J. Appl. Phys. **83**, 358 (1998).
[12] R. F. Schmitsdorf, T. U. Kampen, and W. Mönch, J. Vac. Sci. Technol. B **15**, 1221 (1997).
[13] F. E. Jones, B. P. Wood, J. A. Myers, C. Daniels-Hafer, and M. C. Lonergan, J. Appl. Phys. **86**, 6431 (1999).
[14] M. H. Hecht, L. D. Bell, W. J. Kaiser, and F. J. Grunthaner, Appl. Phys. Lett. **55**, 780 (1989).
[15] C. Detavernier, R. L. Van Meirhaeghe, R. Donaton, K. Maex, and

F. Cardon, J. Appl. Phys. **84**, 3226 (1998).
[16] A. Olbrich, J. Vancea, F. Kreupl, and H. Hoffmann, Appl. Phys. Lett. **70**, 2559 (1997).
[17] H.-J. Im, Y. Ding, J. P. Pelz, B. Heying, and J. S. Speck (unpublished).
[18] W. J. Kaiser and L. D. Bell, Phys. Rev. Lett. **60**, 1406 (1988); L. D. Bell and W. J. Kaiser, *ibid.* **61**, 2368 (1988).
[19] B. J. Skromme, E. Luckowski, K. Moore, M. Bhatnagar, C. E. Weitzel, T. Gehoski, and D. Ganser, J. Electron. Mater. **29**, 376 (2000).
[20] H.-J. Im, B. Kaczer, J. P. Pelz, and W. J. Choyke, Appl. Phys. Lett. **72**, 839 (1998).
[21] In this article SBH is measured as electric potential barrier of an electron and thus has dimension of volts. Also the term ''potential'' used here refers to negative of the real electric potential.
[22] S. M. Sze, *Physics of Semiconductor Devices*, 2nd ed. (Wiley, New York, 1981).
[23] U. Karrer, O. Ambacher, and M. Stutzmann, Appl. Phys. Lett. **77**, 2012 (2000).
[24] $n_{if} \cong (1+\partial\Delta\phi/\partial V)^{-1}$ is due to the Schottky effect (Ref. 22), where the image force induces the barrier lowering, $\Delta\phi$. This is only a mild effect for our system ($n_{if}<1.02$ for $V<0.75$ V) because the 6*H*-SiC epilayer used is weakly doped.
[25] L. J. Schowalter and E. Y. Lee, Phys. Rev. B **43**, R9308 (1991).
[26] K. Reuter, F. J. Garcia-Vidal, P. L. de Andres, F. Flores, and K. Heinz, Phys. Rev. Lett. **81**, 4963 (1998).
[27] H. Sirringhaus, E. Y. Lee, and H. von Känel, Phys. Rev. Lett. **73**, 577 (1994); T. Meyer and H. von Känel, *ibid.* **78**, 3133 (1997).
[28] P. R. Bevington, *Data Reduction and Error Analysis for the Physical Sciences* (McGraw-Hill, New York, 1969), p. 242.
[29] Notice small difference in notations between this article and Ref. 8: (1) The number density of patches c_1 used here accounts for both lower and higher potential patches (of equal number) and is twice as big as that in Ref. 8. (2) A negative value of γ is meaningful in this article and represents a higher potential patch. (3) The effective area $A_{\text{patch}}(\gamma)$ defined here is different from A_{eff} in Ref. 8.
[30] $(E_C-E_F)_{\text{neutral}}$ for the 6*H*-SiC sample used in this study is calculated to be 0.24 eV using the conduction band density-of-state effective mass for electrons $m_{de}/m_0=0.70$. See Ref. 4 and Ref. 22, p. 17.
[31] Strictly speaking, $P_p[\phi_B]$ is defined only for positive values of ϕ_B and, therefore, is not exactly Gaussian. However the effect of the deviation may be safely neglected.
[32] An even better, almost perfect, fit could be obtained if ϕ_B^0 is also allowed to change by a small amount (a few hundredths of a volt smaller than $\langle\phi_B^{\text{local}}\rangle_{\text{good}}$).